J Therm Anal Calorim
DOI 10.1007/s10973-012-2673-z

Influence of amorphous block on the thermal behavior of well-defined block copolymers based on ε-caprolactone

Mario D. Ninago · Angel J. Satti · Andrés E. Ciolino · Marcelo A. Villar

Received: 29 June 2012 / Accepted: 30 August 2012

Abstract In this work, we studied the thermal characterization of block copolymers based on ε-caprolactone. The copolymers were obtained by anionic polymerization techniques, using different co-monomers such as styrene (S) and dimethylsiloxane (DMS). Synthesized copolymers were characterized by H-nuclear magnetic resonance, size exclusion chromatography, and Fourier transform infrared spectroscopy. Isothermal crystallization was performed by differential scanning calorimetry (DSC), and Avrami's theory was employed in order to obtain kinetics parameters of interest, such as the half-life for the crystallization process ($t_{1/2}$), the bulk crystallization constant (k), and the Avrami's exponent (n). The spherulitic growth was measured by polarized optical microscopy in order to determine the crystallization behavior. Poly(ε-caprolactone) block (PCL) crystallization was analyzed by considering the physico-chemical characteristics of the neighboring block, PS or PDMS. The chemical nature of the neighbor block in the PCL-based copolymer affects the kinetics parameters of Avrami's equation, as can be deduced by comparing the values obtained for pure PCL and the studied block copolymers. On the other hand, the apparent thermal degradation activation energies E_{ad} for PCL and block copolymers were determined by Ozawa's method. The incorporation of PDMS instead of PS improves the stability of the resulting copolymer, as it was observed by thermogravimetric analysis.

M. D. Ninago (✉) · A. J. Satti · A. E. Ciolino · M. A. Villar
Planta Piloto de Ingeniería Química (PLAPIQUI), Departamento de Ingeniería Química, Universidad Nacional del Sur (UNS), Consejo Nacional de Investigaciones Científicas y Técnicas (CONICET), Camino "La Carrindanga" Km 7, 8000 Bahía Blanca, Argentina
e-mail: mninago@plapiqui.edu.ar

Keywords Copolymers · Isothermal crystallization · Poly(ε-caprolactone) · Poly(styrene) · Poly(dimethylsiloxane)

Introduction

Block copolymers are useful materials with several interesting applications. Different properties can be obtained by combining blocks from different monomers, each one with different chemical properties. Over the past few decades, a significant amount of research has been carried out mainly focusing on AB diblock or ABA triblock copolymers [1]. In particular, semi-crystalline block copolymers usually show richness in morphology due to the competition between microphase separation and crystallization. This behavior is determined by the segregation strength as well as by the morphology. As it was pointed out by Xu and Zheng [2], block copolymers with strong segregation strength can lead to confined crystallization, and thus the morphology in the melt is preserved after crystallization. On the other hand, block copolymers with weak segregation strength may result in breakout crystallization, and lamellar structure is formed in the solid irrespective of the morphology in the melt. In the last decades, block copolymers based on poly(ε-caprolactone) (PCL) have received a considerable interest because of their potential applications in medical devices, pharmaceutical controlled release systems, degradable packaging materials, implantable biomaterials, and microparticules for drug delivery, among others [3–8]. PCL is a hydrophobic, semi-crystalline polymer. Its low melting point of approximate 60 °C has allowed preparing blends with different natural polymers for different applications [9–11]. On the other hand, the combination of two or more blocks of structurally

Published online: 21 September 2012

different polymers can be used to obtain materials with specific properties, such us chemical resistance, impact strength, flexibility or weatherability.

The crystallization behavior of a block copolymer containing at least one semicrystalline block is not only of theoretical interest for understanding polymer morphology, but also of basic importance in practical operations of polymer transformation such as extrusion and melt spinning among others. Previous studies on the influence of amorphous polymers on the crystallization behavior of crystalline polymers have been reported, and the presence of an amorphous polymer in PCL blend results in a reduction in the growth rate of spherulites [12–20]. The crystallization and melting behavior of crystalline polymers are often affected by the presence of other components. It is well established that structural parameters such as lamellar thickness, crystal interphase, and spherulitic growth rates are substantially modified by other components. Isothermal crystallization kinetics can adequately be described by Avrami's analysis, which remains as the most popular method for obtaining information on crystallization kinetics. On the other hand, Ozawa's analysis can be used to determinate the degradation process of the copolymers. Both methods provide qualitative information about kinetic parameters, which should be complemented by microscopic investigations.

Crystalline morphology in polymer thin films can display unusual patterns such as complex ring bands or dendrites instead of regular Maltese cross spherulites. The patterns can be further influenced by factors such as film thickness, temperature range, or the presence of amorphous diluent polymers [18]. Patterns of crystalline spherulites in polymers will depend on the structure, geometry restriction during growth, or crystallization temperature among others. Crystallization kinetics and spherulite growth mechanism have been extensively studied on semicrystalline polymers, such as poly(ε-caprolactone) (PCL) or their blends with amorphous polymers. Influencing factors may include weight average molar mass (M_W), mass fractions, miscibility, and copolymer or blend composition [19, 20].

The objective of this work is to investigate the isothermal crystallization kinetics of PCL homopolymer and copolymers. The crystallization kinetics for pure PCL is investigated as a function of crystallization temperature, T_c; to find a suitable value of T_c to understand the effect of the presence of amorphous blocks, such as PS and PDMS on the crystallization kinetics of PCL block. Spherulitic growth in films and transformation of spherulitic patterns in different crystallization regimes were investigated by comparing the copolymers with PCL homopolymer.

Materials and methods

Materials

Solvents and monomers used for the synthesis of block copolymers were purified according to conventional anionic polymerization standards [21–23]. Linear model block copolymers were synthesized by using *sec*-butyllithium (*sec*-Bu^-Li^+) as initiator, which was freshly prepared in vacuum from *sec*-butyl chloride (Fluka) and lithium metal (Fluka). Diphenylethylene (DPE) was purified under vacuum, distilled from calcium hydride and fractionated in glass-sealed ampoules. Tetrahydrofuran (THF, Ciccarelli) was used as promoter of hexamethylcyclotrisiloxane monomer (D_3) polymerization, whereas cyclohexane (Dorwill) and degassed methanol (Química Industrial) were used as solvent and terminating agent, respectively. D_3 and styrene (S) monomers (Sigma-Aldrich) were purified according to the conventional routines of high-vacuum anionic polymerization techniques. ε-caprolactone monomer (ε-CL, Aldrich) was purified by distillation in vacuum from calcium hydride. Freshly distilled glass-sealed ampoules of each pure monomer, or diluted in benzene were collected and stored at −20 °C prior to use.

Copolymerization reactions

The synthesis of model block copolymers studied in this work (PS-*b*-PCL and PDMS-*b*-PCL) was carried out under high vacuum by sequential addition of monomers, in glass Pyrex® reactors equipped with break-seals for the addition of the reagents, and constrictions for removal of products at different reaction stages [24, 25]. Depending on the desired bock copolymer, different living macroinitiators were employed to obtain the PCL block. The addition product between DPE and living poly(styryl) lithium chains was used as initiator for the anionic ring opening polymerization of ε-CL in PS-*b*-PCL copolymers, whereas living poly(dimethylsiloxanyl) lithium chains were used as initiator to obtain the corresponding PDMS-*b*-PCL copolymers.

Characterization

Nuclear magnetic resonance (^{1}H-NMR)

Nuclear magnetic resonance (^{1}H-NMR) spectra of the copolymers obtained were recorded on a Bruker 300 MHz instrument using deuterated chloroform (Aldrich) as solvent. The composition of copolymers was obtained using the integrated areas of characteristic ^{1}H signals of each monomer.

Size exclusion chromatography (SEC)

Polymer samples were characterized by size exclusion chromatography (SEC) on a system built with a Waters 515 HPLC pump and a Waters model 410 differential refractometer detector, equipped with three mixed bed Phenogel linear (2) columns and a pre-column with 5 μm bead size (Phenomenex). The solvent employed was toluene flowing at a rate of 1 mL min^{-1}. The injection volume was 200 μL, and polystyrene (PS) standards were used for calibration. The Mark-Houwink calibration constants used for each polymer were $K_{PS} = 0.012$ mL g^{-1}, $\alpha_{PS} = 0.71$ for PS, and $K_{PDMS} = 0.0136$ mL g^{-1}, $\alpha_{PDMS} = 0.69$ for PDMS [26]. PCL samples were characterized with the same equipment and set of columns in $CHCl_3$ at 1 mL min^{-1}, using PS standards for calibration, with the following constants: $K_{PS} = 0.0049$ mL g^{-1}, $\alpha_{PS} = 0.794$ for PS [26], and $K_{PCL} = 0.01298$ mL g^{-1}, $\alpha_{PCL} = 0.828$ for PCL [27].

Fourier transform infrared spectroscopy (FTIR)

Fourier transform infrared spectroscopy (FTIR) spectra of the synthesized model block copolymers were obtained on a Nicolet® FTIR 520 spectrometer. Cast films from copolymer solutions (1 wt % in chloroform) were obtained onto NaCl windows. FTIR spectra were recorded at 4 cm^{-1} resolution over the 4,000–400 cm^{-1} range, using an accumulation of 20 scans and air as the background.

Differential scanning calorimetry (DSC)

Differential scanning calorimetry (DSC) was performed on a Pyris 1 Perkin-Elmer® equipment. Samples were measured under nitrogen atmosphere for crystallization experiments and under helium atmosphere for T_g. Temperature and heat of fusion were calibrated by using pure indium metal as a standard reference. Approximately, 0.01 g of each model polymer was employed. The isothermal crystallization analysis was carried out by using the following procedure. First, the sample was heated from 30 to 90 °C at 10 °C min^{-1}. Then, it was kept at 90 °C during 5 min and was rapidly cooled (60 °C min^{-1}) to the selected crystallization temperatures for the PCL block (T_c) according to the methodology reported in the literature [28]. Isothermal crystallization experiments were carried out for temperatures between 40 and 48 °C, by using steps of 2 °C. Finally, after isothermal crystallization, all samples were heated up to 90 °C (10 °C min^{-1}) in order to obtain the heat of fusion (ΔH_f). In all cases, heat of crystallization (ΔH_c) as a function of time (t) was recorded at different isothermal crystallization temperatures (T_c). On the other hand, T_g values were obtained from the second heating using 10 °C min^{-1} as heating and cooling rate.

Polarized optical microscopy (POM)

The morphological development and spherulitic size of PCL and PCL block in the copolymers were also studied by polarized optical microscopy (POM). A Karl Zeiss Pol-III microscope equipped with a JVC video camera and a heating plate was employed. Samples were analyzed by heating at 90 °C for 10 min, and then holding at 40 °C to observe the crystallization growth process.

Thermogravimetric analysis (TG)

Thermal stability of the copolymers was studied in a TGS-2 Perkin-Elmer® balance. Weight was recorded between 35 and 600 °C at a heating rate of 10 °C min^{-1} under nitrogen flow. To determine the influence of PS or PDMS block in the thermal stability of PCL block, copolymers with similar molar masses and chemical composition were tested. From the analysis of the curves obtained, the apparent thermal degradation activation energy E_{ad} for PCL homopolymer, and PCL-based block copolymers was determined by employing Ozawa's method [29].

Results and discussion

Chemical characterization of PS-*b*-PCL and PDMS-*b*-PCL

The linear model block copolymers studied were obtained by anionic polymerization (high-vacuum techniques) using sequential addition of monomers. To achieve this, careful experimental conditions were employed in order to obtain a good control of each block. Table 1 summarizes the molecular and thermal characterization done by SEC, DSC, and ^{1}H-NMR for both series of block copolymers.

Synthesized block copolymers exhibit different CL content (ranging from 5 to 80 wt%), and narrow molar mass distributions ($M_w/M_n < 1.2$). Among them, PDMS-*b*-PCL copolymers exhibit higher polydispersity indexes than PS-*b*-PCL copolymers series. This fact should deserve a better experimental study; by the moment, we can only suggest that these apparently "higher" polydispersity indexes should be attributed to the occurrence of back-biting reactions. As it is reported in the literature, the occurrence of this kind of reactions is typical in the polymerization processes of both ε-CL and D_3 monomers [30]. In such a sense, a more careful study is currently carried out. Figures 1 and 2 show the FTIR spectra of PCL, PS, and PDMS homopolymers, and their respective block copolymers. In both figures, spectra from homopolymers are shifted in the absorbance axis in order to display the common absorption bands that appear in the copolymers.

Table 1 SEC, ^{1}H NMR, and DSC characterization of the synthesized block copolymers

Polymer	M_n^a/g mol^{-1}	M_w/M_n^b	w_{PCL}^c	M_n^d/g mol^{-1}	T_m^e/°C^c	$T_{g(CL)}^f$/°C	X/%^{g}
PCL	11,000	1.14	1	–	56.9	−66.0	44.7
ECL1	68,800	1.01	0.10	77,300	52.7	nd	20.7
ECL2	35,000	1.07	0.45	77,800	54.2	−64.9	40.4
ECL3	101,400	1.04	0.76	133,400	55.3	−65.1	32.9
SCL1	15,000	1.16	0.05	15,700	57.4	nd	22.4
SCL2	52,000	1.23	0.45	95,500	57.3	−65.2	36.5
SCL3	29,300	1.09	0.77	129,800	58.5	−64.8	29.9

[a] M_n of PDMS or PS blocks determined by SEC, [b] polydispersity index of PDMS and PS blocks according to SEC, [c] weight fraction of PCL (w_{PCL}) determined by ^{1}H-NMR, [d] Mn of copolymers (ECL and SCL) according to SEC and ^{1}H-NMR analysis, [e] melting point, [g] glass transition temperature of the PCL block, [g] percentage of crystallinity of PCL block determined by DSC

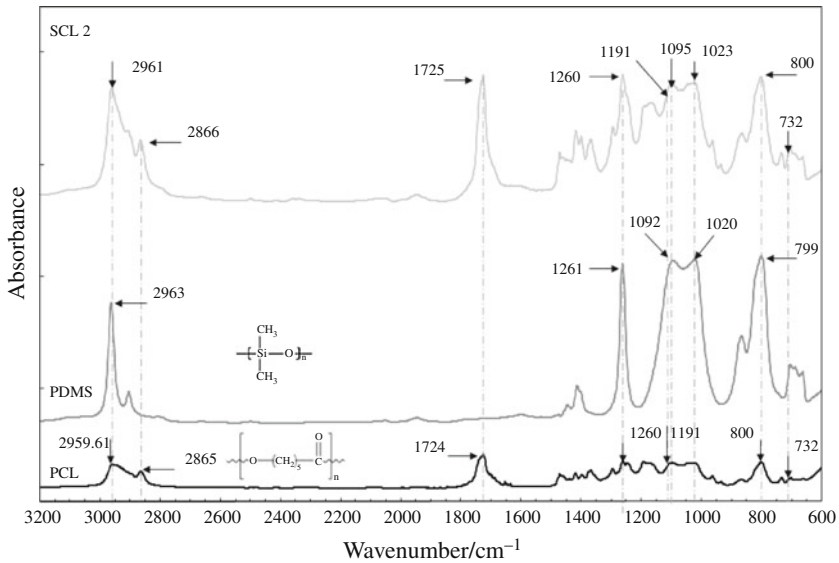

Fig. 1 FTIR spectrum of PCL homopolymer (*black bottom*), PDMS homopolymer (*medium, gray*) and SCL2 copolymer (*top, gray*)

Arrows indicate common bands, and the most significant resemblances between them will be described as follows.

For PCL, characteristics absorptions bands can be observed at 2,960 and 2,865 cm^{-1} corresponding to vibration bands of methylene groups (ν_{CH}). At 1,724 cm^{-1}, the spectrum displays a strong and acute band due to the stretching vibrations of the carbonyl groups ($\nu_{C=O}$) [31]. At 1,260 and 1,191 cm^{-1}, weak bands appear resulting from the stretching vibration of O–C=O bonds, and at 732 cm^{-1} appears a small band attributed to the bending vibration of the methylene groups $(–CH_2–)_n$ with $n > 4$. The spectrum of PDMS homopolymer displays an absorption band at 2,963 cm^{-1} which corresponds to out of phase vibrations of the C–H bonds of methyl groups (ν_{CH}). At 1,261 cm^{-1}, it can be noticed the absorption band corresponding to the out of phase vibrations of Si–$(CH_3)_2$ and O–Si–OR bonds. At 1,092, 2,010, and 799 cm^{-1} appear the absorption bands corresponding to symmetric vibration of Si–O–Si bonds, and out of phase vibrations of C–Si–C bonds. For the copolymer SCL 2, the characteristic absorption bands of each block can be easily noticed and compared with the corresponding homopolymers. The PCL semi-crystalline block shows bands at 2,961, 2,866, and 1,725 cm^{-1} which are common with those of PCL homopolymer, whereas the elastomeric block shows bands at 1,260, 1,095, 1,023, and 800 cm^{-1} which are common to those of PDMS homopolymer.

The spectrum of PS homopolymer showed in Fig. 2 displays an absorption band at 3,025 cm^{-1} associated with the vibration of =CH bonds of aromatic rings. The corresponding vibrations of methylene groups appear at 2,851 cm^{-1} (νs CH_2) and at 2,924 cm^{-1} (νa CH_2). At 1,601 and 1,452 cm^{-1}, the absorption bands attributed to C=C bonds can be observed. Finally, mono substituted aromatic compounds show absorption bands at 907 and 698 cm^{-1} (γ = CH).

For the copolymer ECL2, the characteristic absorption bands of each block can be easily observed and compared with those corresponding to the homopolymers. Again, the semi-crystalline PCL block shows bands at 2,926, 2,851, and 1,725 cm^{-1} which are common with those of PCL homopolymer, whereas the vitreous block shows bands at

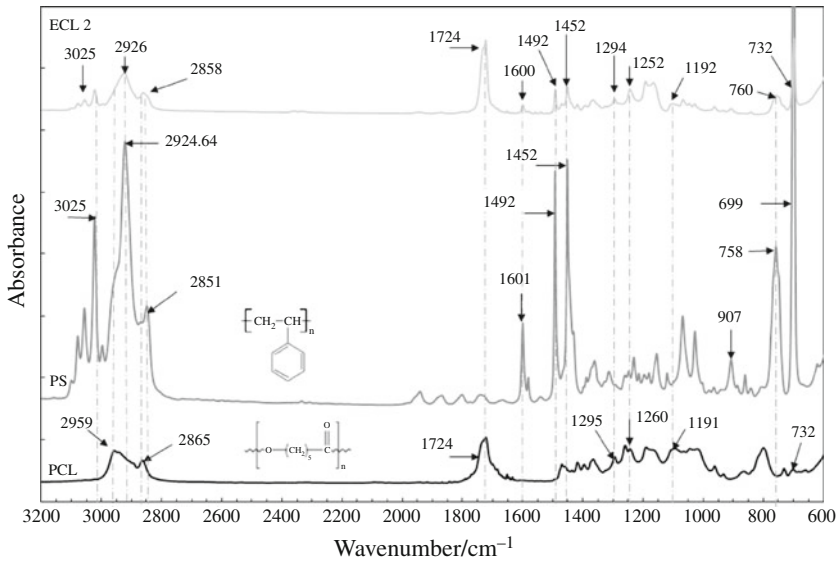

Fig. 2 FTIR spectrum of PCL homopolymer (*bottom, black line*), PS homopolymer (*medium, gray line*), and ECL2 copolymer (*top, gray line*)

3,025, 1,452, 1,252, and 1,192 cm^{-1} which are common with those of PS homopolymer.

Isothermal crystallization employing differential scanning calorimetry (DSC)

Isothermal crystallization experiments of polymers employing differential scanning calorimetry (DSC) can be analyzed using Avrami's equation (1) in order to obtain kinetics parameters of interest such as the half-life for crystallization ($t_{1/2}$), the bulk crystallization constant (k), and the Avrami exponent (n) [32–36].

$$V_c = 1 - \exp(-kt^n) \tag{1}$$

The exponent n represents the type of crystallization and can adopt values of 1, 2, or 3 corresponding to one-, two-, or three-dimensional crystallization; V_c is the relative volumetric fraction of transformed material; and k is the overall crystallization rate constant. The volumetric fraction of crystalline PCL (V_c) can be calculated as:

$$V_c = \frac{w_c}{w_c + (\rho_c/\rho_a)(1 - w_c)}, \tag{2}$$

where ρ_c and ρ_a are the density of fully crystalline and fully amorphous PCL, respectively [34], and w_c is the crystalline mass fraction that can be calculated as

$$w_c = \frac{\Delta H_t}{\Delta H_\infty}, \tag{3}$$

where ΔH_t is the enthalpy value for the amount of transformed material at time t and ΔH_∞ is the maximum enthalpy value reached at the end of the isothermal crystallization process (t_∞) [37–39].

Then, Eq. (1) can be re-written by applying logarithms to both sides. The following expression is obtained:

$$\log[-\ln(1 - V_c)] = \log k + n \log t \tag{4}$$

Figure 3 shows the experimental isothermal crystallization kinetics data for PCL at different crystallization temperatures (T_c). After maintaining the sample for 5 min at 90 °C, it was cooled down at 60 °C min^{-1} to the crystallization temperature and the isothermal step was immediately started. The induction time (which includes the stabilization time) has been named t_0 and it was obtained by drawing a horizontal line from a point after the crystallization process has finished to a point at the beginning of the crystallization curve (Fig. 3) following the methodology reported in the literature [28]. An increase in T_c shifts the exothermic peak to longer times, the peak becomes flatter, and there is an increase in the time to reach the maximum degree of crystallization.

By plotting $\log[-\ln(1 - V_c)]$ versus $\log t$ (Eq. 4), the Avrami's exponent n and the overall crystallization rate constant k can be obtained. The resulting linear plots of isothermal crystallization data along with the linear regression for ECL2 are showed in Fig. 4. From these curves, the half-time of crystallization $t_{1/2}$, defined as the time required for half of the final crystallinity to be developed, can be obtained. Usually, $t_{1/2}$ is directly used to characterize the rate of crystallization. The higher the value of $t_{1/2}$, the smaller is the rate of crystallization. From those fits, the type of crystallization for PCL homopolymer and PCL block in the copolymers studied was determined. Block copolymers show a two-dimensional crystallization regime, with Avrami's exponent values between 1.6 and 2.7. The crystallization of the PCL block was analyzed considering the presence of an amorphous block (PDMS or PS) at the crystallization temperature of the PCL block. Table 2 summarizes the kinetics parameters obtained from isothermal crystallization experiments. Kinetics parameters were obtained employing the following equation [40]

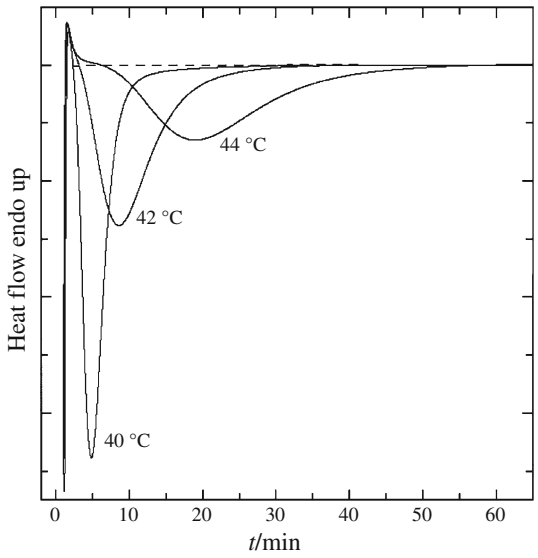

Fig. 3 Isothermal DSC scans of PCL at different crystallization temperatures (T_c). The sample was maintained at 90 °C for 5 min and then cooled at 60 °C min^{-1} to the isothermal crystallization temperature T_c

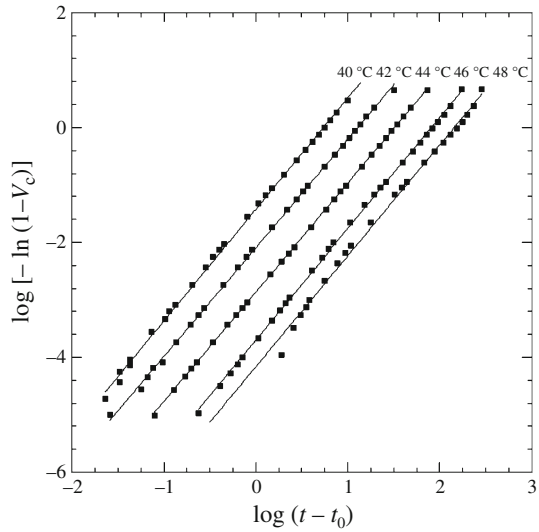

Fig. 4 Experimental data obtained from the isothermal crystallization of ECL2 at different crystallization temperature (T_c). *Solids lines* represent Avrami's equation fit for each temperature

$$\frac{1}{n}(\ln K) = \ln K_0 - \frac{E_a}{RT_c} \tag{5}$$

where K_0 is a temperature-independent pre-exponential factor, E_a is the activation energy; and R is the universal gas constant. Plots of n^{-1} ln K versus T_c^{-1} for PCL, and the copolymers are linear, and E_a can be determined from the slope.

Figure 5 shows the evolution of $t_{1/2}$ at each crystallization temperature (T_c) studied. For all the crystallization temperatures employed, PDMS block is amorphous, and PS block is glassy. For the copolymers studied, Avrami's exponent n were lower (1.9–2.2) than the value obtained for PCL homopolymer (2.2–2.6). The values of $t_{1/2}$ for all copolymers are similar to pure PCL for crystallization temperatures in the range of 40–44 °C (Fig. 5). However, a difference in $t_{1/2}$ values appears for crystallization temperatures closer to T_m. Half-life values at crystallization temperatures of 46 and 48 °C are a function of block copolymer composition. Block copolymers with lower contents of either PDMS or PS in a PCL matrix (SCL3 and ECL3) show $t_{1/2}$ values higher than pure PCL. On the other hand, block copolymers with contents of either PDMS or PS higher than that of PCL (SCL1, SCL2, and ECL2) present $t_{1/2}$ values lower than pure PCL. Values of activation energy (E_a) are shown in Table 2.

Glass transition temperature (T_g) values obtained for the PCL block in the copolymers are similar to the corresponding value for PCL homopolymer. On the other hand, copolymers with a PDMS block, except SCL1, showed values of E_a similar to PCL homopolymer, whereas copolymers with a PS block presented lower values of E_a compared to the PCL. These results indicate that the state (glassy or amorphous) of the block attached to the PCL block (PS or PDMS) modifies the values of E_a. Copolymers having a PDMS block (SCL), have E_a values similar to the PCL homopolymer indicating that the presence of an amorphous block ($T_{g\ PDMS} \ll T_c$) does not affect the crystallization of PCL block. On the other hand, copolymers with a PS block showed lower E_a values compared with the value obtained for PCL homopolymer, probably associated with a lower mobility of PCL due to the attached glassy PS block ($T_{g\ PS} > T_c$). Similar results were reported for PCL blends with inorganic fillers [40].

Isothermal crystallization employing polarized optical microscopy (POM)

When a polymer crystallizes from concentrated solutions, or by subcooling from the molten state, large aggregates with spherical morphology (spherulites) are developed. The Lauritzen–Hoffman theory [41] can be used to predict the spherulitic grow rate (G) as a function of the crystallization temperature (T_c), which can be expressed by the secondary nucleation theory of polymer growth [41–43] as follows:

$$G(T) = G_0 \exp\left[-\frac{U^*}{R(T_c - T_\infty)}\right] \exp\left[-\frac{K_g}{T_c \Delta T f}\right] \tag{6}$$

$$f = \frac{2T_c}{T_c + T_m^0} \tag{7}$$

where U^* is the activation energy of the transport process, K_g is the secondary nucleation constant, G_0 is an empirical

Table 2 Values of $t_{1/2}$ (min), n, k, and E_a at different crystallization temperatures (T_c) for PCL, PS-*b*-PCL, and PDMS-*b*-PCL copolymers

	T_c/°C					
	40	42	44	46	48	E_a/kJ mol^{-1}
PCL						
$t_{1/2}$	3.6	7.8	18.4	46.8	91.0	342.8
n	2.2	2.1	2.4	2.6	2.4	
k	4.1×10^{-2}	9.1×10^{-3}	7.1×10^{-4}	3.5×10^{-5}	1.3×10^{-5}	
ECL2						
$t_{1/2}$	4.1	7.6	14.5	29.2	40.0	232.5
n	1.9	1.9	1.9	1.9	1.9	
k	4.7×10^{-2}	1.6×10^{-2}	4.6×10^{-3}	1.8×10^{-3}	5.8×10^{-4}	
ECL3						
$t_{1/2}$	4.5	10.5	14.0	67.0	118.8	287.4
n	1.9	1.9	1.9	1.9	1.9	
k	3.4×10^{-2}	8.1×10^{-3}	1.4×10^{-3}	2.0×10^{-4}	6.9×10^{-5}	
SCL 1						
$t_{1/2}$	6.3	10.3	11.5	26.5	46.6	217.4
n	1.7	1.6	1.6	1.8	2.1	
k	3.3×10^{-2}	1.9×10^{-2}	1.2×10^{-2}	1.0×10^{-3}	2.5×10^{-4}	
SCL2						
$t_{1/2}$	1.1	1.6	3.1	7.6	26.2	327.5
n	2.7	2.2	2.1	2.1	2.2	
k	3.7×10^{-1}	2.5×10^{-1}	6.5×10^{-2}	1.1×10^{-2}	5.9×10^{-4}	
SCL3						
$t_{1/2}$	4.2	8.4	18.1	42.3	121.7	346.5
n	1.9	2.0	2.1	2.1	2.2	
k	4.5×10^{-2}	1.1×10^{-2}	1.8×10^{-3}	2.3×10^{-4}	1.8×10^{-5}	

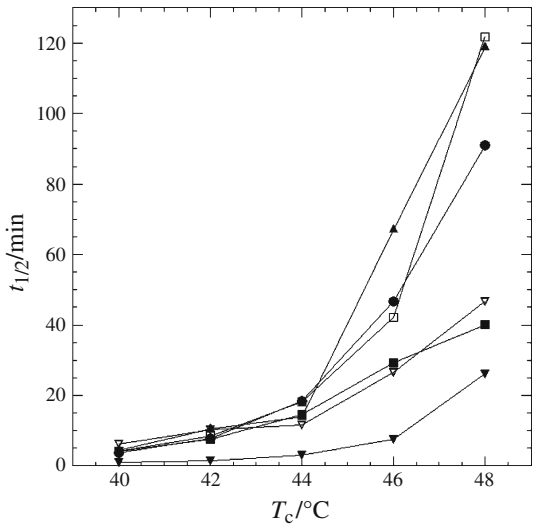

Fig. 5 Dependence of $t_{1/2}$ with the isothermal crystallization temperature (T_c). *Filled circle* PCL, *open inverted triangle* SCL1, *filled square* ECL2, *filled inverted triangle* SCL2, *open square* SCL3, *and filled triangle* ECL3

constant, which includes those factors independent of temperature, T_c is the crystallization temperature, and T_∞ is the temperature at which molecular motion ceases (usually T_g −30 K) [44]. $\Delta T = \left(T_m^0 - T_c\right)$ is the degree of subcooling, T_m^0 is the melting temperature at equilibrium [42], and f is a correction factor that considers the change in melting enthalpy with temperature. The nucleation constant K_g can be expressed as:

$$K_g = \frac{n_e b_0 \sigma \sigma_e T_m^0}{\Delta H^0 k}, \tag{8}$$

where n_e is a constant equal to 4 for regime I and III, and 2 for regimen II, b_0 is the thickness of the monolayer in the direction normal to the growth plane, σ is the lateral-surface free energy, k is the Boltzman constant, and ΔH^0 is the thermodynamic enthalpy of melting. Rewriting Eq. 6 in a logarithmic form results in:

$$\ln G + \frac{U^*}{R(T_c - T_\infty)} = \ln G_0 - \frac{K_g}{T_c \Delta T f} \tag{9}$$

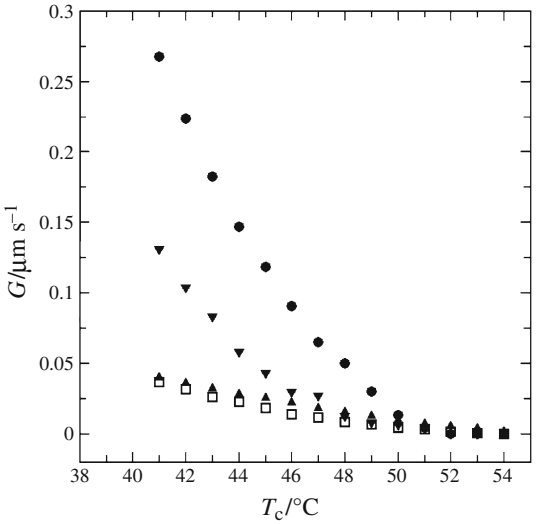

Fig. 6 Crystal growth rates for PCL and its copolymers at different crystallization temperatures. *Filled circle* PCL, *filled inverted triangle* SCL2, *open square* ECL3, and *filled triangle* SCL3

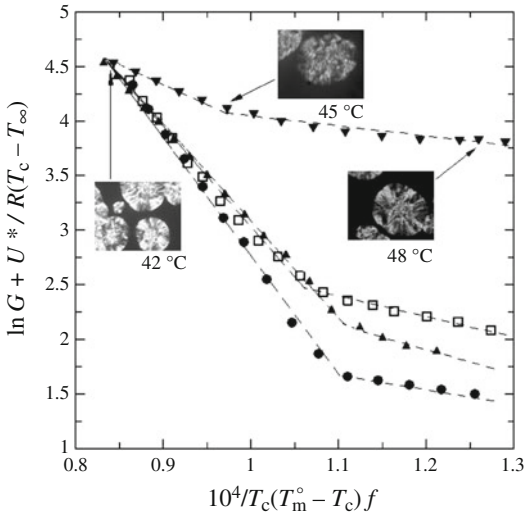

Fig. 7 Lauritzen-Hoffman representation for PCL homopolymer and its copolymers employing $U^* = 6{,}276$ J mol^{-1}. *Filled circle* PCL, *filled inverted triangle* SCL2, *open square* ECL3, and *filled triangle* SCL3

Then, K_g can be obtained by plotting the left-hand side of Eq. 9 as a function of $(T_c \Delta T f)^{-1}$.

Results indicate that morphology does not change in the range of temperatures studied. By plotting the spherulitic radius as a function of time for each crystallization temperature (T_c), a linear dependence is observed. Therefore, we can assume that spherulitic growth is independent of the radius. Then, spherulitic growth ratio was calculated by the slope of the experimental radius versus time. Figure 6 shows the spherulitic growth rates for PCL and for the copolymers at different crystallization temperatures, T_c. PCL homopolymer shows the highest growth rate compared with the copolymers. Similar results were reported in the literature for PCL and PCL blends [40, 45–49].

Experimental data were also used to plot the Lauritzen–Hoffman expression (Eq. 9). Figure 7 shows regimens II and III for PCL homopolymer and the copolymers. For PCL homopolymer multiple nucleations occurs on the same layer along the whole sample in the range of 40–45 °C. At the transition temperature between regimes II and III ($T_c \approx 46.5$ °C), the spherulites obtained showed a not well-defined texture or a dendritic fibrillar type, and crystals with different sizes. At crystallization temperatures above 46 °C, the size of the spherulites increases and crystallization can be characterized by regime II. On regime III, there is a simultaneous growth of all cores and all crystals start growing at the same time (athermal nucleation). On the other hand, in regimen II, the crystals start growing sporadically throughout the crystallization time (thermal nucleation). For SCL2 copolymer, regimes II and III can be observed. At crystallization temperatures below 45 °C, spherulites obtained have a fibrillar texture, with the characteristic Maltese cross, as shown in the photograph taken at $T_c = 42$ °C (Fig. 7). At the transition temperature ($T_c \approx 45.5$ °C), the spherulites obtained did not show a clearly defined texture, whereas at higher crystallization temperatures spherulites with a larger fibrillar appearance and regions with a dendritic structure are observed. For copolymers ECL3 and SCL3 a simultaneous growth of the cores is observed along the entire surface analyzed (regime III). At higher crystallization temperatures, a fibrillar texture with the characteristic Maltese cross is observed. Similar results were obtained by Chen and Wu [39] in blends of PS/PCL with a transition temperature from regime II to III at 48 °C, close to the value obtained for the copolymers analyzed in this study (≈47.5 °C) for similar compositions.

The crystallization rate of PCL block in the copolymers is different to PCL homopolymer. However, all the materials show regimes II and III in the range of crystallization temperature studied. Table 3 shows K_g values obtained for each sample in both regimes, the relationship between the nucleation constants, and the transition temperature between regime II and III. K_g values obtained in this work are similar to those reported in the literature for PCL-based materials [45, 46].

Crystallization constant ratio (K_g^{III} / K_g^{II}) values obtained are in the range of 1.7–2.8 for all samples analyzed. These results are similar to those reported in the literature [40] and consistent with Lauritzen–Hoffman theory, where the predicted ratio is equal to 2.

Thermogravimetric analysis (TG)

Mass changes of the sample can be evaluated as a function of temperature (dynamic method), where the temperature

Table 3 Kinetic values obtained from polarized microscopy measurement for regime calculations to PCL and its copolymers

Copolymer	w_{PCL}	K_g^{III}/K^{-2}	K_g^{II}/K^{-2}	K_g^{III}/K_g^{II}	$T_{III} \rightarrow T_{II}/^{\circ}C$
PCL	1.00	115,100	51,200	2.25	46.5
SCL2	0.45	33,900	12,300	2.76	45.5
SCL3	0.78	102,000	40,800	2.50	47.5
ECL3	0.76	81,800	47,900	1.71	47.5

increases linearly according to a heating program. To determine the kinetic parameters that characterize this change, we applied a kinetic study of the degradation process [29]. Thermogravimetric analysis (TG) of copolymers was used to obtain mass changes between 35 and 600 °C, in order to determine how the presence of the amorphous block (PS or PDMS) affects the thermal stability of PCL block. Experiments were performed with copolymers of similar molar mass and composition. From the analysis of the curves obtained, the initial degradation temperature was determined.

TG analysis was also used to obtain the degradation kinetics of PCL and its copolymers. Figure 8 shows TG curves for SCL2 and ECL2 copolymers, obtained at different heating rates ($\beta = 5$, 10, 20, and 40 °C min^{-1}). Then, the degree of conversion (α) at a given temperature was obtained from the curves.

Figure 8b shows two steps in the degradation curve for the copolymer SCL2. The first part of the curve (between 100 and 50 % mass loss) could be attributed to the degradation of PCL, and the second part corresponds to the degradation of the PDMS block. In the case of the copolymer ECL2 (a), which has a PS block attached to the PCL chain, just one step was observed in the curve since the value of degradation temperature of PS and PCL are similar. The apparent activation energy of degradation (E_{ad}) was calculated from the slope of logarithm of heating rate (log β) as a function of T^{-1}, at each value of α for PCL and copolymers, using the following expression [29].

$$E_{ad} = -\text{slope}\frac{R}{0.457} \quad (10)$$

where R is the universal gas constant.

PCL homopolymer showed an average activation energy of degradation $E_{ad} = 159$ kJ mol^{-1}, value that agrees with that reported by Abdellatif et al. [44]. The block copolymer with PDMS (SCL2) showed a decrease in the average value ($E_{ad} = 145$ kJ mol^{-1}), and the block copolymer with PS (ECL2) showed an increase ($E_{ad} = 183$ kJ mol^{-1}) in the average activation energy of degradation compared to PCL homopolymer. Figure 9 shows the evolution of the activation energy of degradation (E_{ad}) as a function of the degree of conversion (α). PCL homopolymer and block

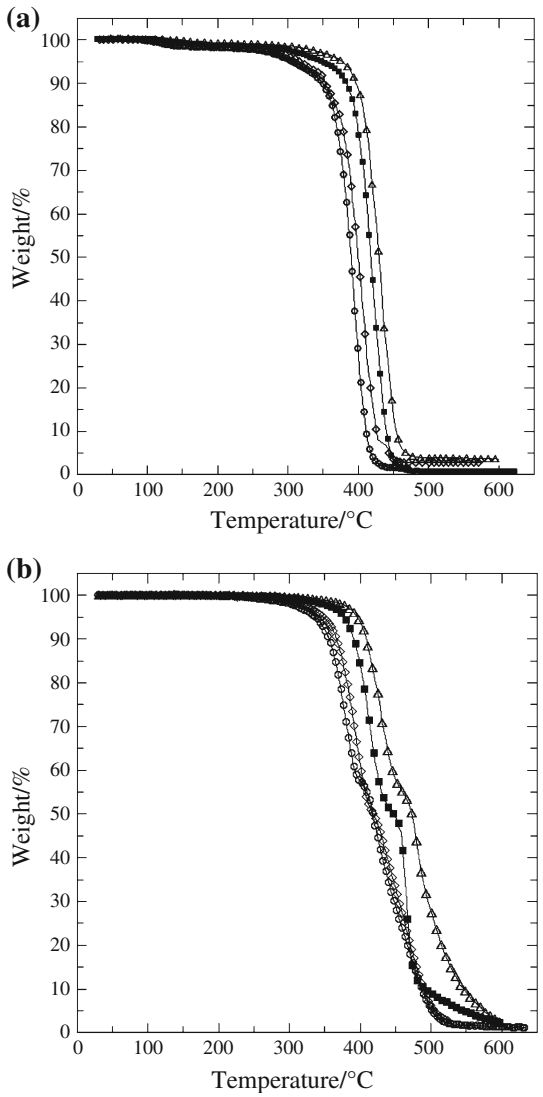

Fig. 8 TG curves for ECL2 (**a**) and SCL2 (**b**). *Open circle* $\beta = 5$ °C min^{-1}, open diamond $\beta = 10$ °C min^{-1}, *open square* $\beta = 20$ °C min^{-1}, and *open triangle* $\beta = 40$ °C min^{-1}

copolymers studied (SCL2 and ECL2) showed two degradation mechanisms: the first one at α values between 0.02 and 0.1 with an initial value of E_{ad} of 76 kJ mol^{-1}; and the second one with an activation energy value almost constant for higher conversion rates ($\alpha = 0.2$–0.9). Values obtained for ECL2 are consistent with those reported in the literature for the degradation of physical blends of PS and PCL, with mass fractions of the components similar to the copolymers studied in this work [50, 51].

Conclusions

PS-*b*-PCL and PDMS-*b*-PCL copolymers with controlled molar mass and low polydispersity indexes were obtained

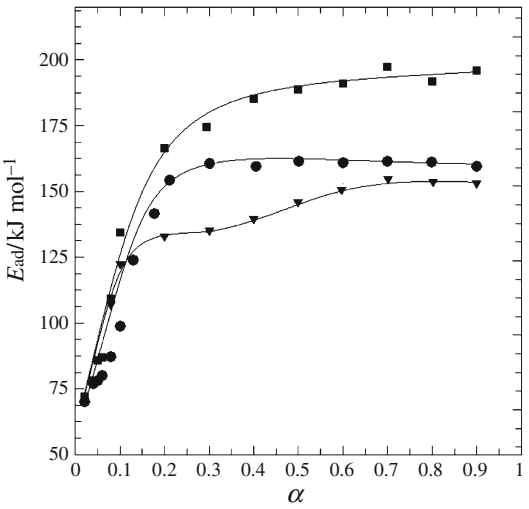

Fig. 9 Deagradation activation energy (E_{ad}) as a function of the degree of conversion (α). *Open circle* PCL, *filled inverted triangle* SCL2, and *filled square* ECL2

by employing anionic polymerization and sequential addition of monomers. The isothermal crystallization kinetic for PCL homopolymer and its copolymers was studied by DSC, and analyzed by using Avrami's equation. Avrami's exponent values (n) obtained for the block copolymers were lower than values obtained for neat PCL homopolymer. On the other hand, values of $t_{1/2}$ for all copolymers were similar to the PCL in the crystallization temperature range of 40–44 °C, but decreased significantly for crystallization temperatures between 46 and 48 °C. Avrami's exponent values obtained were in the range of 1.6–2.7, indicating that PCL block in the copolymers crystallizes in two dimensions (disk and cylindrical).

By using optical microscopy with polarized light, the spherulitic growth was analyzed. The rate of spherulitic growth was adjusted with the Lauritzen–Hoffman model, where the constants of crystallization showed a marked dependence on crystallization temperature in the range of 45–48 °C, in analogy with isothermal crystallization experiments.

Degradation profiles were investigated by TG. For neat PCL and ECL2 copolymer activation energy values were similar to those reported in the literature for PCL and PS/PCL blends. Block copolymers showed two degradation mechanisms. One at low conversion (0.02–0.2), which corresponds to the initial stage of degradation, and a second one at higher conversion values (0.2–0.9). The copolymer with a PDMS block (SCL2) showed an increase in the value of the degradation activation energy, suggesting that this copolymer has a higher thermal resistance to degradation in the initial stage of the process. Furthermore, at higher values of conversion ($\alpha > 0.2$), the activation energy of the degradation decreases. The block copolymer with a PS block (ECL2) showed a value of activation energy similar to PCL homopolymer in the first stage of degradation ($\alpha = 0.02$–0.20), and then an increase in the degradation activation energy for higher conversions ($\alpha > 0.2$).

Acknowledgements We express our gratitude to the Consejo Nacional de Investigaciones Científicas y Técnicas de la República Argentina (CONICET), the Agencia Nacional de Promoción Científica y Tecnológica (ANPCyT), and the Universidad Nacional del Sur (UNS, Argentina) for their financial support for this study.

References

1. Hamley I. The physics of block copolymers. New York: Oxford University Press; 1998.
2. Xu Z, Zheng S. Morphology and thermomechanical properties of nanostructured thermosetting blends of epoxy resin and poly(ε-caprolactone)-block-polydimethylsiloxane-block- poly(ε-caprolactone) triblock copolymer. Polymer. 2007;21:6134–44.
3. Engelberg I, Kohn J. Physico-mechanical properties of degradable polymers used in medical applications: a comparative study. Biomaterials. 1992;12:292–304.
4. Pulapura S, Kohn X. Trends in the development of bioresorbable polymers for medical applications. J Appl Biomater. 1992;6: 216–50.
5. Heuschen J, Vion J, Jêrome R. Polycaprolactone-based block copolymers. 3. Mechanical behavior of diblock copolymers of styrene and ε-caprolactone. Macromolecules. 1989;22:2446–51.
6. Broz ME, Vander Hart DL, Broz ME, Washburn NR. Structure and mechanical properties of poly(D,L-lactic acid)/poly(ε-caprolactone) blends. Biomaterials. 2003;24:4181–9.
7. Contreras RJ, Carrillo M, Balsamo V, Torres C, Carrasqueño L. Estudio preliminar de la síntesis secuencial y caracterización de terpolímeros ABC basados en isopreno, estireno y ε-caprolactona. Revista Latinoamericana de Metalurgia y Materiales. 2007;1: 41–51.
8. Ludueña LN, Alvarez VA, Vázquez A. Processing and microstructure of PCL/clay nanocomposites. Mater Sci Eng A. 2007; 460:121–9.
9. Woodruff MA, Hutmacher DW. The return of a forgotten polymer polycaprolactone in the 21st century. Prog Polym Sci. 2010; 35:1217–56.
10. Atanase LI, Glaied O, Riess G. Crystallization kinetics of PCL tagged with well-defined positional triazole defects generated by click chemistry. Polymer. 2011;52:3074–81.
11. Alfonso GC, Russell TP. Kinetics of crystallization in semicrystalline amorphous polymer mixtures. Macromolecules. 1986; 19:1143–52.
12. Defieuw G, Groeninckx G, Reinares G. Miscibility, crystallization and melting behaviour, and semicrystalline morphology of binary blends of polycaprolactone with poly(hydroxy ether of bisphenol A). Polymer. 1989;30:2164–9.
13. Kuo SW, Chan SC, Chang FC. Crystallization kinetics and morphology of binary phenolic/poly(ε-caprolactone) blends. J Polym Sci. 2004;42:117–28.
14. Toda A, Taguchi K, Kajioka H. Growth of banded spherulites of poly(ε-caprolactone) from the blends: an examination of the modeling of spherulitic growth. Polymer. 2012;53:1765–71.
15. Shin EJ, Jeong W, Brown HA, Koo BJ, Hedrick JL, Waymouth RM. Crystallization of cyclic polymers: synthesis and crystallizationbehavior of high molecular weight cyclic poly(ε-caprolactone)s. Macromolecules. 2011;8:2773–9.

16. Liu H, Huang Y, Yuan L, He P, Cai Z, Shen Y, Xu Y, Xiong H. Isothermal crystallization kinetics of modified bamboo cellulose/PCL composites. Carbohydr Polym. 2010;79:513–9.
17. Castillo RV, Müller A, Raquez JM, Dubois P. Crystallization kinetics and morphology of biodegradable double crystalline PLLA-*b*-PCL diblock copolymers. Macromolecules. 2010;43:4149–60.
18. Chen YF, Woo EM. Isothermal crystallization kinetics and thermal behavior of poly(ε-caprolactone)/multi-walled carbon nanotube composites. Colloid Polym Sci. 2008;286:917–26.
19. Chen H, Li L, Ou-Yang W, Hwang JC, Wong WY. Spherulitic crystallization behavior of poly(ε-caprolactone) with a wide range of molecular weight. Macromolecules. 1997;30:1718–22.
20. Kressler J, Svoboda P, Inoue T. Influence of copolymer composition on the crystallization in PCL/SAN blends. Polymer. 1993;24:3225–33.
21. Hadjichristidis N, Iatrou H, Pispas S, Pitsikalis M. Anionic polymerization: high vacuum techniques. J Polym Sci Part A. 2000;38:3211–34.
22. Morton M, Fetters L. Anionic polymerization of vinyl monomers. Rubber Chem Technol. 1975;48:359–409.
23. Uhrig D, Mays J. Experimental techniques in high-vacuum anionic polymerization. J Polym Sci Part A. 2005;43:6179–222.
24. Bellas V, Iatrou H, Hadjichristidis N. Controlled anionic polymerization of hexamethyl cyclotrisiloxane. Model linear and miktoarm star, co- and terpolymers of dimethylsiloxane with styrene and isoprene. Macromolecules. 2000;33:6993–7.
25. Ciolino AE, Sakellariou G, Pantazis D, Villar MA, Vallés EM, Hadjichristidis N. Synthesis and characterization of model diblock copolymers of poly(dimethylsiloxane) with poly(1,4-butadiene) or poly(ethylene). J Polym Sci Part A. 2006;44:1579–90.
26. Kurata M, Tsunashima Y. Section VII: solution properties. In: Brandup J, Immergut EH, Grulke EA, editors. Polymer handbook. 4th ed. New York: Wiley; 1999.
27. Sun H, Mei L, Song C, Cui W, Wang P. The in vivo degradation, absorption and excretion of PCL-based implant. Biomaterials. 2006;27:1735–40.
28. Lorenzo AT, Arnal ML, Albuerne J, Müller A. DSC isothermal polymer crystallization kinetics measurements and the use of the Avrami equation to fit the data: guidelines to avoid common problems. Polym Test. 2007;26:222–31.
29. Ozawa T. A new method of analyzing thermogravimetric data. Bull Chem Soc Jpn. 1965;38:1881–6.
30. Ito K, Hashizuka Y, Yamashita Y. Equilibrium cyclic oligomer formation in the anionic polymerization of ε-caprolactone. Macromolecules. 1977;10:821–4.
31. Murphy SH, Leeke GA, Jenkins MJ. A comparison of the use of FTIR spectroscopy with DSC in the characterisation of melting and crystallisation in polycaprolactone. J Therm Anal Calorim. 2012;107:669–74.
32. Childs MA, Matlock DD, Dorgan JR, Ohno TR. Surface morphology of poly(caprolactone)-*b*-poly(dimethylsiloxane)-*b*-poly(caprolactone) copolymers: effects on protein adsorption. Biomacromolecules. 2001;2:526–37.
33. Tang L, Sheu MS, Chu T, Huang YH. Anti-inflammatory properties of triblock siloxane copolymer-blended materials. Biomaterials. 1999;20:1365–70.
34. Kofron W, Baclawski L. A convenient method for estimation of alkyllithium concentrations. J Org Chem. 1976;41:1879–80.
35. Avrami M. Kinetics of phase change. I. General theory. J Chem Phys. 1939;7:1103–12.
36. Hatakeyama T, Quinn FX. Thermal analysis. Fundamentals and applications to polymer science. New York: Wiley; 1994.
37. Gan Z, Jian B, Zhang J. Poly(ε-caprolactone)/poly(ethylene oxide) diblock copolymer. I. Isothermal crystallization and melting behavior. J Appl Polym Sci. 1996;59:961–7.
38. Krikorian V, Pochan D. Unusual crystallization behavior of organoclay reinforced poly(L-lactic acid) nanocomposites. Macromolecules. 2004;37:6480–91.
39. Chen EC, Wu TM. Isothermal crystallization kinetics and thermal behavior of poly(ε-caprolactone)/multi-walled carbon nanotube composites. Polym Degrad Stab. 2007;92:1009–15.
40. Hoffman JD, Weeks J. Melting process and the equilibrium melting temperature of polychlorotrifluoroethylene. J Res Natl Bur Stand A. 1962;66:13–28.
41. Hoffman JD. Role of reptation in the rate of crystallization of polyethylene fractions from the melt. Polymer. 1982;23:656–70.
42. Mandelkern L. Crystallization kinetics of homopolymers: overall crystallization: a review. Biophys Chem. 2004;112:109–16.
43. Papageorgiou GZ, Achilias DS, Bikiaris DN, Karayannidis GP. Crystallization kinetics and nucleation activity of filler in polypropylene/surface-treated SiO_2 nanocomposites. Thermochim Acta. 2005;427:117–28.
44. Abdellatif M, Sherald H, Girma B. Polycaprolactone/polystyrene bioblends characterized by thermogravimetry, modulated differential scanning calorimetry and infrared photoacoustic spectroscopy. Polym Degrad Stab. 2007;92:1177–85.
45. Trujillo M, Arnal ML, Müller AJ, Mujica MA, Urbina de Navarro C, Ruelle B, Bubois P. Supernucleation and crystallization regime change provoked by MWNT addition to poly(ε-caprolactone). Polymer. 2012;53:832–41.
46. Siqueira G, Fraschini C, Bras J, Dufresne A, Prud'homme R, Laborie MP. Impact of the nature and shape of cellulosic nanoparticles on the isothermal crystallization kinetics of poly(ε-caprolactone). Eur Polym J. 2011;47:2216–27.
47. Sasaki T. Melting of poly(ε-caprolactone) studied by step-heating calorimetry. J Therm Anal Calorim. 2012. doi:10.1007/s10973-012-2209-6.
48. Nanaki SG, Papageorgiou GZ, Bikiaris DN. Crystallization of novel poly(ε-caprolactone)-block-poly(propylene adipate) copolymers. J Therm Anal Calorim. 2012;108:633–45.
49. Sun J, He C, Zhuang H, Jing X, Chen X. The crystallization behavior of poly(ethylene glycol)-poly(ε-caprolactone) diblock copolymers with asymmetric block compositions. J Polym Res. 2011;18:2161–8.
50. Pushkaraj J, Giridhar M. Degradation of polycaprolactone in supercritical fluids. Polym Degrad Stab. 2008;93:1901–8.
51. Balsamo V, Gouveia LM. Estimation of thermodynamic and kinetic secondary nucleation parameters in poly(styrene-co-maleic anhydride)/poly(ε-caprolactone) blends. Revista Latinoamericana de Metalurgia y Materiales. 2010;31:26–34.